Truncated Tetrahedron Seed Crystals Initiating Stereoaligned Growth of FeSi Nanowires

Si-in Kim,[†] Hana Yoon,[†] Kwanyong Seo,[†] Youngdong Yoo,[†] Sungyul Lee,[‡,*] and Bongsoo Kim[†,*]

[†]Department of Chemistry, KAIST, Daejeon 305-701, Korea and [‡]Department of Applied Chemistry, Kyung Hee University, Kyungki 446-701, Korea

ABSTRACT

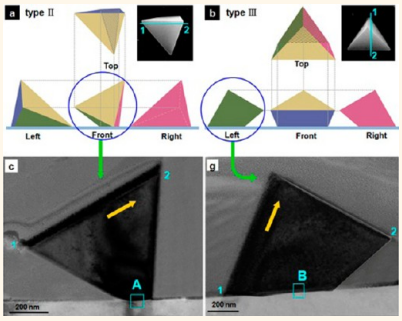

We have synthesized epitaxially grown freestanding FeSi nanowires (NWs) on an *m*-Al_2O_3 substrate by using a catalyst-free chemical vapor transport method. FeSi NW growth is initiated from FeSi nanocrystals, formed on a substrate in a characteristic shape with a specific orientation. Cross-section TEM analysis of seed crystals reveals the crystallographic structure and hidden geometry of the seeds. Close correlation of geometrical shapes and orientations of the observed nanocrystals with those of as-grown NWs indicates that directional growth of NWs is initiated from the epitaxially formed seed crystals. The diameter of NWs can be controlled by adjusting the composition of Si in a Si/C mixture. The epitaxial growth method for FeSi NWs *via* seed crystals could be employed to heteroepitaxial growth of other compound NWs.

KEYWORDS: iron silicide · transition metal silicides · nanowires · epitaxial growth · seed crystal

Metal silicides have a very low resistivity, large optical absorption, excellent figure of merit (*Z*), and unique magnetic properties. These versatile properties in addition to their compatibility with silicon-based device fabrication processes can lead to a wide variety of nanoscale applications of metal silicides in electronics, photovoltaics, thermoelectrics, and spintronics.[1−9] Among the metal silicides, FeSi is a paramagnetic semiconductor that exhibits anomalous temperature-dependent electrical, optical, and magnetic properties and is known as the only transition metal Kondo insulator showing Kondo lattice behavior at room temperature.[10−12]

Growing freestanding nanowires (NWs) in an aligned orientation on a substrate is crucial to the fabrication of three-dimensional device architectures.[13,14] Manufacturing processes of integrated devices can be much simplified by employing self-alignment of NWs as desired. The alignment and orientations of NW arrays can strongly affect device functionality in practical applications.[15,16] While FeSi NWs have been synthesized in various morphologies such as a freestanding form or a hyperbranched form by varying the reaction conditions without any catalysts, the detailed growth mechanism has not been revealed yet.[17−19]

Herein we report catalyst-free epitaxial growth of freestanding FeSi NWs and their detailed growth mechanism. Freestanding metal silicide NWs are epitaxially grown for the first time. The reaction proceeded by chemical vapor transport (CVT) without any catalysts. The NW growth is initiated from the FeSi nanocrystals, formed on a substrate in a characteristic shape with a specific orientation at an initial stage of synthesis. Close correlation of geometrical shapes and orientations of the observed nanocrystals with those of as-grown NWs indicates that directional growth of NWs is initiated from the epitaxially formed seed crystals on the substrate. Interestingly, the heteroepitaxial growth mechanism of compound NWs observed here is quite close to the mechanism of catalyst-free epitaxial growth of noble metal NWs,[20−22] although *via* more complex-shaped seed crystals. Investigation of epitaxial growth of FeSi NWs may help us to understand the growth mechanism of other compound NWs, especially semiconductor NWs, without using a catalyst.

RESULTS AND DISCUSSION

Stereoaligned Growth of FeSi NWs from Oriented Seed Crystals. Epitaxially aligned FeSi NW arrays were synthesized on an *m*-Al_2O_3 substrate

* Address correspondence to bongsoo@kaist.ac.kr, sylee@khu.ac.kr.

Received for review May 14, 2012 and accepted September 11, 2012.

Published online September 11, 2012
10.1021/nn302141w

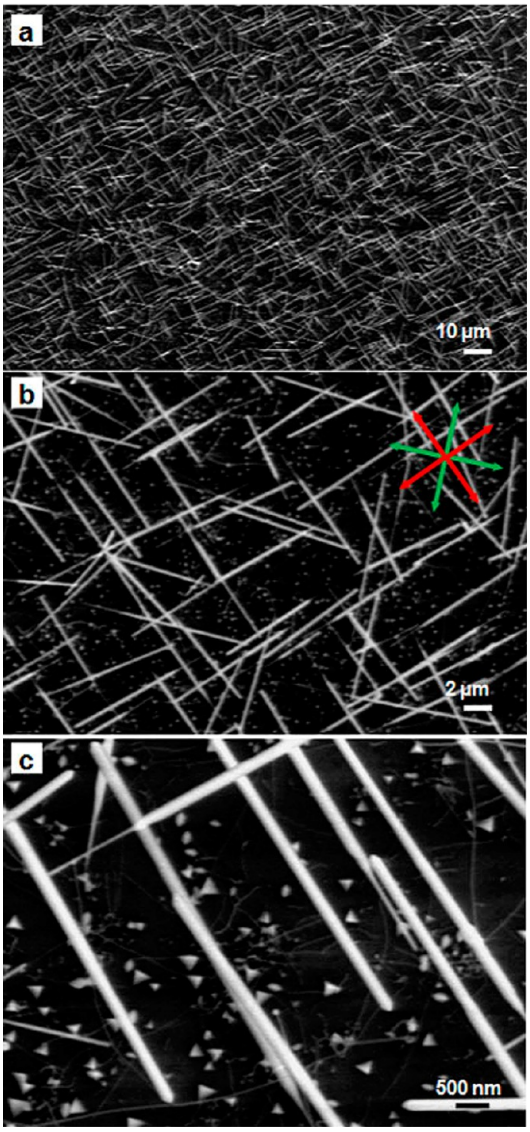

Figure 1. (a–c) SEM images of the epitaxially grown FeSi NWs on an *m*-Al_2O_3 substrate. Red and green arrows in (b) indicate eight growth directions of NWs. (c) Enlarged image shows tetrahedron-shaped nanocrystals with a specific orientation. A large number of nanocrystals are found together with the NWs on the substrate.

using a CVT method without catalysts employing a hot wall dual-zone furnace with a 1 in. diameter quartz tube. As a Fe precursor, anhydrous $FeCl_2$ beads in an alumina boat were placed at a heating zone. The *m*-Al_2O_3 substrates were put on an alumina boat, filled with a powdered Si/C mixture with a 1:8 weight ratio of Si:C, and placed at ~12 cm downstream from $FeCl_2$ (Figure S1, Supporting Information).

Figure 1 shows top-view scanning electron microscope (SEM) images of directionally aligned FeSi NWs on an *m*-Al_2O_3 substrate. Freestanding NWs have eight growth directions, as indicated by the red and green arrows in Figure 1b. Note that small nanocrystals are observed on the substrate in an enlarged SEM image (Figure 1c). The curly NWs with cubic-FeSi phase are also found on the substrate in addition to the presence of straight NWs (Figure S2, Supporting Information).

The X-ray diffraction (XRD) pattern indicates that all peaks correspond to the reflections of a simple cubic FeSi phase (space group $P2_13$, JCPDS card No. 38-1397) with a lattice constant of 4.488 Å (Figure S3, Supporting Information). Transmission electron microscope (TEM) analysis of as-grown NWs also indicates that the NW has a simple cubic FeSi structure, and TEM energy dispersive X-ray spectroscopy (EDS) measurements confirm the Fe:Si composition of 1:1 for the NWs (Figure S4, Supporting Information). A high-resolution TEM (HRTEM) image of a FeSi NW along the $[1\bar{1}0]$ zone axis reveals that a (001) twin plane exists in the middle of the NW along its [110] growth direction. No diffraction spot splitting is observed in its selected area electron diffraction (SAED) pattern. Such an observation in the twinned crystals, quite different from typical twinning behaviors, is ascribed to merohedral twinning, as recently reported by Szczech *et al.* in the FeSi NWs.[19]

For the growth mechanism of the epitaxial FeSi NWs, we suggest a vapor–solid growth mechanism, where building blocks are supplied from the gas phase by direct adsorption onto the NW surface or by diffusion following adsorption onto the substrate.[20] A vapor–liquid–solid mechanism could be ruled out, since no metal catalysts were employed.

We found a number of nanocrystals as well as stereoaligned FeSi NWs on the substrate after the reaction was completed (Figure 1c). Figure 2a shows a top view image of the FeSi nanocrystals showing three distinct shapes, type I, II, and III, aligned in several specific orientations. Figure 2b–d display enlarged top-view SEM images of seed crystals of type I, II, and III, respectively. All the top-view images in Figure 2 were taken at the same fixed angle. We found FeSi NWs that grew in very closely correlated shapes and orientations with the three nanocrystals, as shown in Figure 2e–g and h–j, respectively, showing the tip and root parts of those NWs. For all of observed NW growth directions, we could find seed crystals having the correlated orientation. From this observation we suggest that the epitaxial FeSi NWs are grown from the seed crystals along the dashed line, as shown in Figure 2b–d.

The type I and II seeds in Figure 2b,c are mirror symmetric to each other and of a truncated tetrahedron shape, while that of the type III seed in Figure 2d is close to a regular tetrahedron. Seeds of each type have four orientations, each rotated by about every 90°, leading to a total of 12 orientations (Figure 3c,d). Since the root part has a shade while the tip part shows clear contrast (Figure 2f,i), we can clearly determine the NW growth direction. Figure 2b,c show that the growth directions of the NWs initiated from type I and II seeds are tilted ~45° from the symmetry plane in a top view.

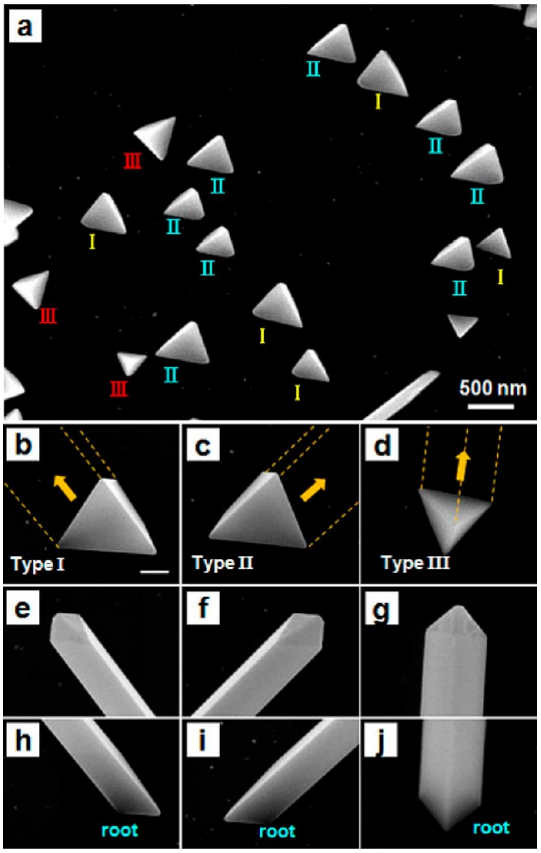

Figure 2. (a) Top-view SEM image of tetrahedron FeSi nanocrystals in various shapes formed on the substrate. The roman numerals near the nanocrystals indicate the geometrical type of nanocrystal as shown in (b−d). (e−g; h−j) Magnified top-view SEM images of tip and root parts of NWs grown from three types of seeds, respectively. Particularly, the root parts show close correlation with three types of seed crystals in geometry and orientations, indicating that NWs grow from seed crystals along the yellow arrows in (b−d). Scale bar in (b) is 200 nm, and (b−j) are all at the same magnification.

Therefore, all four growth directions from type I seed overlap with those from type II seed, and we found a total of eight growth directions, four from type I and II seeds and four from type III seeds. The reason that the seeds have four orientations each rotated by 90° will be discussed later.

Morphology Study of Seed Crystals by Cross-Section TEM Analysis. To thoroughly investigate the epitaxial relationship between the FeSi NW and the substrate as well as the crystallographic structure and morphology of the seed crystals, we carried out detailed cross-section TEM analysis of seeds of types II and III (type I and II seeds are mirror-symmetric). From the cross-section TEM image and the top-view SEM image, we have constructed the projection views for a 3D image of type II and III seed crystals in Figure 4a,b, respectively. We represent some side-view images of type II and III seeds obtained at various angles, which is approximately parallel to the projection views shown in Figure 4a,b (Figure S5, Supporting Information). Figure 4c

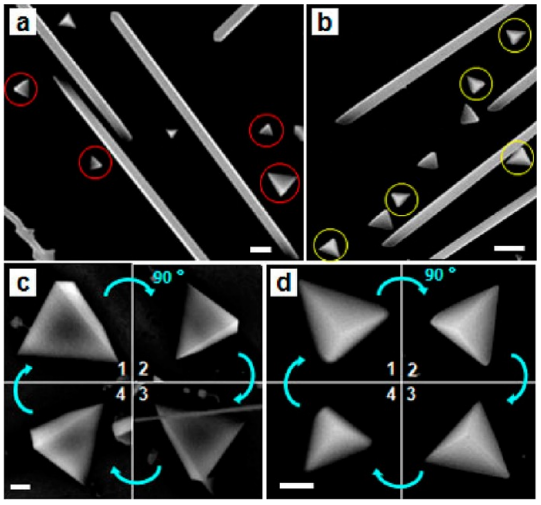

Figure 3. Top-view SEM images of the seed taken at a fixed angle. (a) Seeds of types I and II are formed on the substrate in four orientations rotated by ~90°, as marked by the red circles. (c) Magnified images of the type I seeds in four orientations. (b) Type III seeds have four orientations rotated by ~90°, as marked by the yellow circles. (d) Magnified images of the type III seeds in four orientations. Scale bars in (a, b) and (c, d) are 500 and 200 nm, respectively.

shows a cross-section TEM image of a type II seed, cut along the cyan line (Figure 4a, inset). The cutting plane is carefully selected to be parallel to the NW growth direction and vertical to the substrate (see Figure 2b−d). The quadrangular cross-section TEM image in Figure 4c reveals two additional planes of the type II seed that were hidden in the top-view image. This cross-section image corresponds to the front view in the projection views (blue circle in Figure 4a). Figure 4d displays an HRTEM image of the interface between the type II seed and the *m*-Al_2O_3 substrate (square A in Figure 4c). Figure 4e,f show fast Fourier transform (FFT) electron diffraction (ED) patterns of the seed crystal and the substrate, respectively. The corresponding SAED patterns of Figure 4e,f are displayed in Figure S6a,b (Supporting Information). The diffraction spots from the seed (Figure 4e) are indexed to a simple cubic FeSi structure. From the analysis of the HRTEM image and FFT ED pattern in Figure 4d−f, the lattice mismatch between the ⟨211⟩ direction of a type II seed and the $\langle 11\bar{2}6\rangle$ direction of the *m*-Al_2O_3 substrate was ~13.5%. In a domain matching scheme, however, six lattice constants of FeSi are matched with seven of Al_2O_3 along the FeSi ⟨211⟩ direction with only a 1.94% misfit.

Figure 4g shows a cross-section TEM image of a type III seed, cut along the cyan line (Figure 4b, inset). Although this quadrangular cross-section image looks similar to that in Figure 4c, actual 3D geometrical shapes of the type II and III seeds constructed from the top-view images and the cross-section are quite different, as visualized by the projection views in Figure 4a,b. This is because the cutting planes of the cross-section (insets of Figure 4a,b) are distinctly

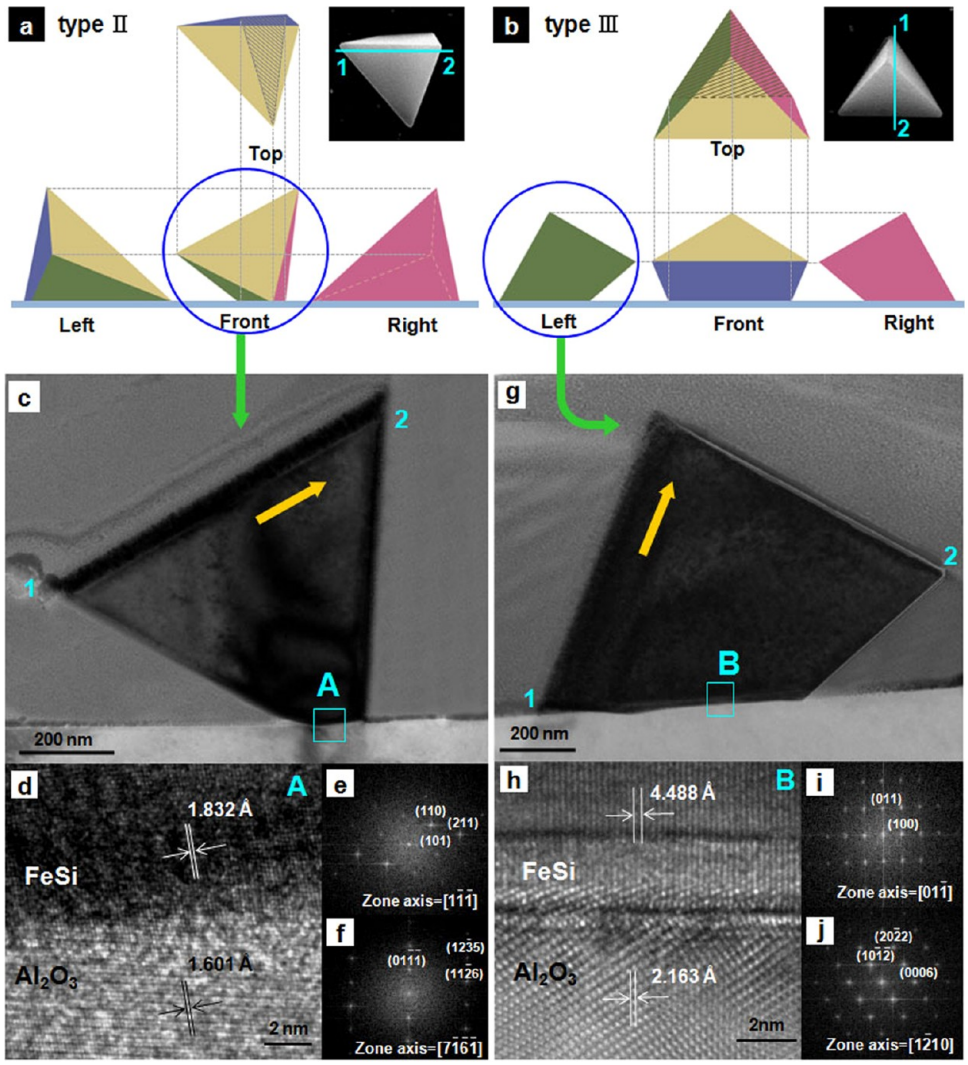

Figure 4. (a, b) Geometry of type II and III seed crystals described by projection views. (Inset images: top-view SEM images of each seed and the cyan line representing the cutting line.) The shaded section of the top view represents the bottom interface with the substrate. (c) Cross-sectional TEM image of a type II seed cut along the cyan line from point 1 to point 2 in the inset of (a). This seed crystal leads to the NW growth along the yellow arrow. (d) HRTEM image of the cyan square A in (c) showing the interface between the type II seed and the substrate. (e, f) FFT ED patterns of the FeSi seed and *m*-Al_2O_3 shown in (d), respectively. (g) Cross-sectional TEM image of a type III seed cut along the cyan line from point 1 to point 2 in the inset of (b). The yellow arrow indicates the NW growth direction from this seed. (h) HRTEM image of the cyan square B in (g). (i, j) FFT ED patterns of the FeSi seed and *m*-Al_2O_3 shown in (h), respectively.

different. The cross-section in Figure 4g corresponds to the left view in the projection views (blue circle in Figure 4b) because the cutting plane here is perpendicular to that of Figure 4c. An HRTEM image of the type III seed/Al_2O_3 interface (square B in Figure 4g) is shown in Figure 4h. FFT ED patterns of the seed and substrate are displayed in Figure 4i,j, respectively. The corresponding SAED patterns of Figure 4i,j are displayed in Figure S6c,d (Supporting Information). The FFT ED pattern of a type III seed matches well to a simple cubic FeSi structure. These analyses of HRTEM images and FFT ED pattern indicate that the epitaxial relationship between the type III seed and the *m*-Al_2O_3 substrate is (110) FeSi//(10$\bar{1}$0) Al_2O_3 (Figure 4i,j). The lattice mismatch is 37.9% between the ⟨100⟩ direction of a type III seed and the ⟨0001⟩ direction of Al_2O_3. The lattice mismatch is 29.2% between the ⟨01$\bar{1}$⟩ direction of a type III seed and the ⟨1$\bar{2}$10⟩ direction of Al_2O_3. In domain matching epitaxy, three lattice constants of FeSi are matched with four of Al_2O_3 along the FeSi ⟨110⟩ direction with a 1.25% misfit, and 10 lattice constants of FeSi are matched with seven of Al_2O_3 along the FeSi ⟨100⟩ direction with a 0.1% misfit (Figure S7a, Supporting Information).

Now we discuss the four observed orientations of the seeds. Since the *m*-Al_2O_3 substrate has a 2-fold symmetry in the crystal atom distribution, the crystal can sit on the substrate in two equivalent orientations rotated by 180°. Figure S7a represents the atomic configuration of the type III seed and Al_2O_3 interfacing each other as in Figure 4h. When the FeSi lattice is rotated by 90° with respect to the substrate, the fine

lattice match is still retained (Figure S7b, Supporting Information). This analysis could explain that the type III seed crystals have four orientations rotated by 90°. Although we do not have lattice matching information for type I and II seeds, they may have similar energetic factors favoring such 90° rotated orientations. Figure 3c,d indicate that four orientations (1, 2, 3, and 4) of type I and III seeds have rotation angles slightly different from 90°, which may be attributed to the more complicated crystal lattice energy factors.

The SEM and TEM investigations suggest that the growth of stereoaligned FeSi NWs is initiated from the FeSi nanocrystals epitaxially formed on a substrate with a characteristic shape and a specific three-dimensional orientation at the beginning of the reaction. Information on the structure and orientation of seed crystals at the initial growth stage of NWs is crucial to elucidate the growth mechanism.[20−22] While the growth mechanism of metal silicide NWs has been extensively investigated, the initial stages of their synthesis have not been revealed in detail yet.[19,23,24] The study on the self-seeded growth of FeSi NWs would provide important clues to understanding the stereoaligned growth of compound NWs without catalysts.

FeSi NWs are also epitaxially grown on *r*-Al_2O_3 substrates (Figure S8, Supporting Information). Unlike the NWs grown on *m*-Al_2O_3 substrates, they have six orientations, as indicated by the red arrows. Seed nanocrystals are also observed on the *r*-Al_2O_3 substrate. Although the lattice mismatch for the FeSi seed and *m*-Al_2O_3 interface is large (38% and 29%), such a sizable lattice mismatch might have acted favorably for the seed formation.[25] Simulation studies predict that for heteroepitaxial thin film formation a small lattice mismatch of ~2% causes film formation, while a large misfit strain of 6% induces semispherical island formation. If the misfit strain is large, adatoms tend to climb to the top of a 3D island instead of covering the substrate surface in order to reduce elastic strain energy, driving rapid growth of 3D islands.

For our FeSi NWs, similarly, Fe and Si atoms preferred to adsorb on top of the seed rather than on the substrate surface because of large lattice mismatches at the interface between the FeSi nanocrystal and the substrate. Thus, we suggest that the epitaxial FeSi NW growth process consists of three steps: First, the vapor phase building blocks originated from precursors condense and diffuse on an Al_2O_3 substrate. Second, after FeSi clusters are aggregated at an initial stage, FeSi seed nanocrystals are formed by adding more Fe and Si atoms. Finally, FeSi NW grows from the FeSi seed. We also suggest that the unique geometries of type II and III seeds reflect an effort to accommodate the large lattice mismatch in the FeSi (type II and III)/Al_2O_3 interface. Additional study is required to reveal the cause of the complicated geometrical shape of the seeds.

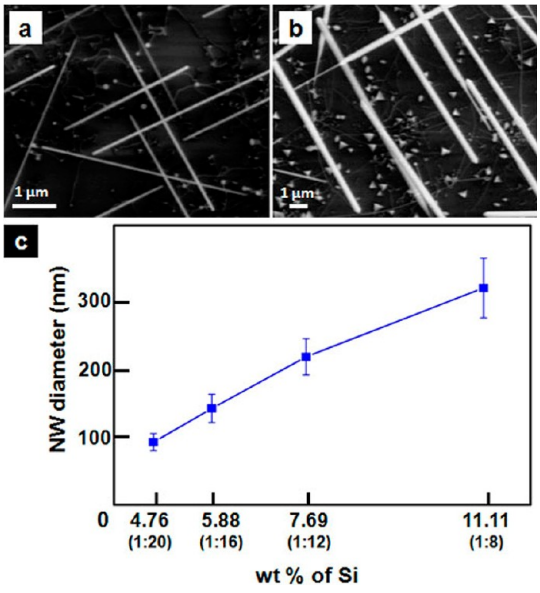

Figure 5. (a, b) SEM images of epitaxially grown FeSi NWs synthesized with the Si:C composition weight ratio of 1:20 and 1:8, respectively. The diameter of NWs in (a) is much smaller than that in (b). (c) Dependence of the NW diameter on Si:C composition ratio of the Si/C mixture.

Control of NW Diameters by Precursor Composition Adjustment. For epitaxial growth of aligned FeSi NWs, substrate temperature and Si vapor pressure have to be optimally adjusted. Since control of Si vapor pressure is quite difficult when a Si substrate is employed as a Si source,[23] we introduced a Si/C powdered mixture and optimized the Si vapor pressure by adjusting the Si:C composition ratio. When Si:C = 1:5 in weight ratio for a Si/C powdered mixture, epitaxial FeSi NWs with a rough surface were synthesized. When the Si:C weight ratio was lowered to 1:8, epitaxial FeSi NWs with a smooth surface were synthesized (Figure 5b). When the Si:C weight ratio was decreased to 1:20, thinner NWs with a smooth surface were synthesized (Figure 5a). Except for the Si:C composition, all other reaction conditions were kept the same. TEM analysis shows that synthesized FeSi NWs have the same B20 simple cubic structure (Figure S9, Supporting Information). Figure 5c illustrates that the diameter of FeSi NWs decreases as the composition of Si in the Si/C mixture decreases. In Fe_xSi_y alloys, the composition of *x*:*y* = 1:1 is thermodynamically the most stable. Since the Fe precursor supply rate is fixed during the reaction, the Si vapor pressure will limit the nucleation and growth rate of the FeSi seeds when the concentration of Si is less than Fe. This explains the observed pressure dependence of the NW diameter on the Si:C composition.

CONCLUSION

In summary, we have synthesized stereoaligned FeSi NWs on an *m*-Al_2O_3 substrate without any catalysts. The FeSi NWs were grown from three kinds of truncated tetrahedron FeSi nanocrystals epitaxially formed

on the substrate. The specific orientations of seed crystals lead to aligned growth of FeSi NWs in several directions. The detailed mechanism of such self-seeded growth was revealed for the first time in metal silicide NW growth. The diameters of the FeSi NWs were modulated by varying the composition ratio in the Si/C powdered mixture. Investigation of self-seeded epitaxial growth of FeSi NWs may help us to understand the growth mechanism of other compound NWs in a specific alignment without using catalysts.

METHODS

Synthesis. Epitaxially grown FeSi NWs were synthesized in a horizontal hot-wall two-zone furnace with a 1 in. diameter inner quartz tube, as shown in Figure S1 (Supporting Information). The setup was equipped with pressure and mass flow controllers. The upstream (US) zone and downstream (DS) zone were used for vaporization of precursor and NW growth, respectively. Anhydrous $FeCl_2$ beads (99.9% purity, Sigma-Aldrich) in an alumina boat used as a Fe precursor were placed at the center of the US heating zone. The FeSi NWs were grown on a rectangular *m*-Al_2O_3 substrate (5 mm × 5 mm) placed on a mixture of Si (99.9% purity, Sigma-Aldrich) and carbon (99.9% purity, Alfa) powder employed as a Si source. The composition ratio of the powdered Si/C mixture was varied in the range 1:8−1:20 to adjust the diameter of the NWs. The substrates were placed at ∼12 cm downstream from the Fe precursor. The carrier Ar gas was supplied through a mass-flow controller at a rate of 200 sccm. The temperatures of the US zone and DS zone were maintained at 530 and 950 °C, respectively, for 20 min of reaction time, while the pressure was maintained at 760 Torr during the reaction. No catalyst was used.

Characterization. XRD patterns of the specimen were recorded on a Rigaku D/max-rc (12 kW) diffractometer operated at 30 kV and 60 mA with filtered Cu Kα radiation. Field emission scanning electron microscope images of FeSi NWs were taken on a Phillips XL30S. TEM and HRTEM images, SAED patterns, and EDS spectra were taken on a JEOL JEM-2100F transmission electron microscope operated at 200 kV. After nanostructures were dispersed in ethanol, a drop of the solution was put on a holey carbon coated copper grid for TEM analysis.

Conflict of Interest: The authors declare no competing financial interest.

Acknowledgment. This research was supported by KRF (S.L.: Converging Research Center Program 2011-K000721, B.K.: 2012-0000648). TEM analyses were performed at KBSI in Daejeon.

Supporting Information Available: Detailed descriptions of supplementary figures. This material is available free of charge *via* the Internet at http://pubs.acs.org.

REFERENCES AND NOTES

1. Kim, J. D.; Anderson, W. A. Direct Electrical Measurement of the Self-Assembled Nickel Silicide Nanowire. *Nano Lett.* **2006**, *6*, 1356–1359.
2. Chang, C. M.; Chang, Y. C.; Ahung, Y. A.; Lee, C. Y.; Chen, L. J. Synthesis and Properties of the Low Resistivity $TiSi_2$ Nanowires Grown with TiF_4 Precursor. *J. Phys. Chem. C* **2009**, *113*, 17720–17723.
3. Chueh, Y. L.; Ko, M. T.; Chou, L. J.; Chen, L. J.; Wu, C. S.; Chen, C. D. $TaSi_2$ Nanowires−A Potential Field Emitter and Interconnect. *Nano Lett.* **2006**, *6*, 1637–1644.
4. Murarka, S. P. Silicide Thin Films and Their Applications in Microelectronics. *Intermetallics* **1995**, *3*, 173–186.
5. Maeda, Y.; Umezawa, K.; Hayashi, Y.; Miyake, K.; Ohashi, K. Photovoltaic Properties of Ion-Beam Synthesized β-$FeSi_2$/n-Si Heterojucntions. *Thin Solid Films* **2001**, *381*, 256–261.
6. Aoyama, I.; Kaibe, H.; Rauscher, L.; Kanda, T.; Mukoujima, M.; Sano, S.; Tsuji, T. Doping Effects on Thermoelectric Properties of Higher Manganese Silicides (HMSs, $MnSi_{1.74}$) and Characterization of Thermoelectric Generating Module using *p*-Type (Al, Ge and Mo)-Doped HMSs and *n*-Type $Mg_2Si_{0.4}Sn_{0.6}$ Legs. *Jpn. J. Appl. Phys.* **2005**, *44*, 4275–4281.
7. Schmitt, A. L.; Higgins, J. M.; Jin, S. Chemical Synthesis and Magnetotransport of Magnetic Semiconducting $Fe_{1-x}Co_xSi$ Alloy Nanowires. *Nano Lett.* **2008**, *8*, 810–815.
8. Manyala, N; Sidis, Y.; Ditusa, J. F.; Aeppli, G.; Young, D. P.; Fisk, Z. Large Anomalous Hall Effect in a Silicon-Based Magnetic Semiconductor. *Nature* **2004**, *3*, 255–262.
9. Hung, M.-H.; Wang, C.-Y.; Tang, J.; Lin, C.-C.; Hou, T.-C.; Jiang, X.; Wang, K. L.; Chen, L.-J. Free-Standing and Single-Crystalline $Fe_{1-x}Mn_xSi$ Nanowires with Room-Temperature Ferromagnetism and Excellent Magnetic Response. *ACS Nano* **2012**, *6*, 4884–4891.
10. Paschen, S.; Felder, E.; Chernikov, M. A.; Degiorgi, L.; Schwer, H.; Ott, H. R. Low-Temperature Transport, Thermodynamic, and Optical Properties of FeSi. *Phys. Rev. B* **1997**, *56*, 12916–12930.
11. Sluchanko, N. E.; Glushkov, V. V.; Demishev, S. V. Crossover in Magnetic Properties of FeSi. *Phys. Rev. B* **2002**, *65*, 064404.
12. Aeppli, E.; Ditusa, J. F. Undoped and Doped FeSi or How to Make a Heavy Fermion Metal with Three of the Most Common Elements. *Mater. Sci. Eng. B* **1999**, *63*, 119–124.
13. Tang, H.; Meng, G.; Huang, Q.; Zhang, Z.; Huang, Z.; Zhu, C. Arrays of Cone-Shaped ZnO Nanorods Decorated with Ag Nanoparticles as 3D Surface-Enhanced Raman Scattering Substrates for Rapid Detection of Trace Polychlorinated Biphenyls. *Adv. Funct. Mater.* **2012**, *22*, 218–224.
14. Fang, X.; Wu, L.; Hu, L. ZnS Nanostructure Arrays: A Developing Material Star. *Adv. Mater.* **2011**, *23*, 585–598.
15. Niu, J. J.; Wang, J. N.; Xu, N. S. 12. Field Emission Property of Aligned and Random SiC Nanowires Arrays Synthesized by a Simple Vapor-Solid Reaction. *Solid State Sci.* **2008**, *10*, 618–621.
16. Fang, X.; Bando, Y.; Ye, C.; Golberg, D. Crystal Orientation-Ordered ZnS Nanobelt Quasi-Arrays and Their Enhanced Field-Emission. *Chem. Commun.* **2007**, *29*, 3048–3050.
17. Ouyang, L.; Thrall, E. S.; Deshmukh, M. M.; Park., H. Vapor-Phase Synthesis and Characterization of ε-FeSi Nanowires. *Adv. Mater.* **2006**, *18*, 1437–1440.
18. Schmitt, A. L.; Bierman, M. J.; Schmeisser, D.; Himpsel, F. J.; Jin, S. Synthesis and Properties of Single-Crystal FeSi Nanowires. *Nano Lett.* **2006**, *6*, 1617–1621.
19. Szczech, J. R.; Jin, S. Epitaxially-Hyperbranched FeSi Nanowires Exhibiting Merohedral Twinning. *J. Mater. Chem.* **2010**, *20*, 1375–1382.
20. Yoo, Y.; Seo, K.; Han, S.; Varadwaj, K. S. K.; Kim, H.; Ryu, J.; Lee, H.; Ahn, J.; Ihee, H.; Kim, B. Steering Epitaxial Alignment of Au, Pd, and AuPd Nanowire Arrays by Atom Flux Change. *Nano Lett.* **2010**, *10*, 432–438.
21. Yoo, Y.; Yoon, I.; Lee, H.; Ahn, J.; Ahn, J. P.; Kim, B. Pattern-Selective Epitaxial Growth of Twin-Free Pd NWs from Supported Nanocrystal Seeds. *ACS Nano* **2010**, *4*, 2919–2927.
22. Yoo, Y.; Han, S.; Kim, M.; Kang, T.; In, J.; Kim, B. Stereoaligned Epitaxial Growth of Single-Crystalline Pt Nanowires by Chemical Vapor Transport. *Chem. Asian J.* **2011**, *6*, 2500–2505.
23. Varadwaj, K. S. K.; Seo, K.; In, J.; Mohanty, P.; Park, J.; Kim, B. Phase Controlled Growth of Metastable Fe_5Si_3 Nanowires by a Vapor Transport Method. *J. Am. Chem. Soc.* **2007**, *129*, 8594–8599.
24. Schmitt, A. L.; Higgins, J. M.; Szczech, J. R.; Jin, S. Synthesis and Application of Metal Silicide Nanowires. *J. Mater. Chem.* **2010**, *20*, 223–235.
25. Guo, J. Y.; Zhang, Y. W.; Lu, C. Effects of Wetting and Misfit Strain on the Pattern Formation of Heteroepitaxially Grown Thin Films. *Comput. Mater. Sci.* **2008**, *44*, 174–179.